Probing the local piezoelectric behavior in stretched barium titanate/poly(vinylidene fluoride) nanocomposites

Anthony Ferri, Sophie Barrau, R. Bourez, Antonio Da Costa, Marie-Hélène Chambrier, Adeline Marin, Juliette Defebvin, Jean Marc Lefebvre, Rachel Desfeux

Version of Record: https://www.sciencedirect.com/science/article/pii/S0266353819325072
Manuscript_9e18cb14f651109e40f8ec2bc4daf692

Probing the local piezoelectric behavior in stretched barium titanate/poly(vinylidene fluoride) nanocomposites

A. Ferri[1,*], S. Barrau[2], R. Bourez[1], A. Da Costa[1], M.-H. Chambrier[1], A. Marin[2], J. Defebvin[2], J.M. Lefebvre[2], R. Desfeux[1]

[1] Université Artois, CNRS, Centrale Lille, ENSCL, Université Lille, UMR 8181, Unité de Catalyse et Chimie du Solide (UCCS), F-62300 Lens, France

[2] Université Lille, Sciences et Technologies, CNRS, ENSCL, INRA, UMR 8207, Unité Matériaux Et Transformations (UMET), F-59655 Villeneuve d'Ascq, France

ABSTRACT

The nanoscale piezoelectric and ferroelectric behavior of barium titanate/poly(vinylidene fluoride) (BT/PVDF) nanocomposite films has been investigated by means of atomic force microscopy (AFM). An uniaxial stretching step was first carried out to promote the polar β crystal phase of the PVDF matrix, as confirmed by infrared spectroscopy and piezoelectric force microscopy (PFM) analysis. Fragmentation of the original polymer crystalline structure upon drawing, as evidenced by the presence of nanometric crystalline blocks did not damage the composite film, thanks to the strong interfacial cohesion between ceramic and polymer brought by nitrodopamine functionalization of the BT inclusions. By scanning the composite surface using PFM, highly piezo-active regions were evidenced and attributed to the BT nanoparticles that could not be identified on the AFM topography images. The precise manipulation of the ferroelectric polarization states in these individual BT grains embedded into the PVDF matrix has

been successfully achieved, confirmed by the local electromechanical deformation simultaneously detected. Reversible switching of the out-of-plane polarization orientation spatially confined into the particles was evidenced. The ability of the contact PFM tool to both directly visualize individual piezoelectric nanofillers dispersed into a polymer matrix and monitor the polarization states is demonstrated, thus highlighting the versatility of PFM for the advanced characterization of electroactive nanocomposites.

KEYWORDS: PVDF; $BaTiO_3$; Piezoelectricity; Ferroelectricity; Atomic force microscopy.

1. INTRODUCTION

During the past decade, an increasing effort was brought to the development of functional ceramic-polymer composites owing to the beneficial impact on specific properties, such as high dielectric constant and breakdown field, low permittivity loss, mechanical flexibility and weight reduction when both components are associated. Based on such functional composites, numerous innovative high performance devices have reached the market such as sensors, acoustic transducers, micro/nano electromechanical systems (MEMS/NEMS) or high-charge storage systems [1,2,3]. In the case of advanced electroactive devices, a commonly privileged strategy is to use a polar polymer matrix filled with piezoelectric inorganic particles [4]. Poly(vinylidene fluoride), PVDF, a semi-crystalline polymer, is widely considered in this approach [5]. PVDF displays five crystal polymorphs (α, β, γ, δ, ε) related to different chain conformations [6]. The non polar α-phase is the more stable, while the polar β-phase exhibits the largest dipolar moment and

thus the better electroactive properties [7,8]. This latter phase may be obtained by stretching a film originally in α-phase [9], by addition of specific nucleants [10,11], by solvent casting [12] or through the synthesis of PVDF copolymers [13]. Introducing piezoelectric ceramic particles with superior dielectric constants ($\varepsilon_r > 10^3$) into polymer matrices, like PVDF-based polymers with ε_r of 10, is a widely-investigated strategy to produce high-performance piezoelectric composites [14,15,16,17,18]. Additionally, chemical functionalization of the ceramic surface was demonstrated to improve the interfacial cohesion between these inclusions and the organic matrix thus ensuring an efficient stress transfer [19,20]. Besides, in a context of environmental concern, piezoelectric inorganic fillers without toxic element are targeted. With the aim to fulfill these requirements Barium Titanate, $BaTiO_3$ (BT) appears as a good candidate owing to its high electromechanical coupling coefficients, excellent dielectric constants and large piezoelectric coefficients up to 460 pC/N in bulk [21]. In this framework, probing the response of such inclusions at the nanoscale is a crucial step for optimizing macroscopic performance of devices based on such piezocomposites. In order to investigate electromechanical phenomena at the nanoscale, advanced modes of atomic force microscopy (AFM) are powerful tools. Some studies were carried out on piezoelectric ceramic-polymer composite materials by means of AFM methods [22,23,24,25,26,27,28]. For example, the switching capability of $BaTiO_3$/P(VDF-TrFE) composites was studied by Valiyaneerilakkal *et al.* by means of piezo-force microscopy (PFM) over micrometric regions [22]. Silibin *et al.* have reported the existence of a broad region (~40 nm) of transient behavior at the interface between P(VDF-TrFE) matrix and barium lead zirconate titanate inclusions, as experimentally assessed by PFM and confirmed by a theoretical approach. It was attributed to inhomogeneous stress

distributions originating from a strong difference between the thermal expansion coefficients of the two components [27]. More recently, Shvartsman *et al.* have reported on the local investigation of (Pb,Ba)(Zr,Ti)O_3 particles incorporated in P(VDF-TrFE) matrix by means of Kelvin probe force microscopy (KPFM) and PFM as a function of temperature [23]. They showed that the discontinuity of the surface potential and the polarization at the interface between inorganic compounds and polymer matrix allowed the study of the evolution of the poled states in these composites.

Nevertheless, to date no direct visualization associated to polarization manipulation of individual piezoelectric nanofillers incorporated into a piezoelectric polymer matrix have been described. Along these lines, the present study deals with the characterization of the nanoscale piezoelectric and ferroelectric behavior of stretched BT/PVDF nanocomposites by means of the PFM technique. In particular, the spontaneous electromechanical response and the ferroelectric polarization control of single BT nanoparticles functionalized with nitrodopamine are investigated. It is worth noting that the choice of PVDF as the polymer matrix instead of P(VDF-TrFE) further bring the opportunity to assess by PFM the coexistence in the stretched composite of both the β polar phase as well as the non polar α phase.

2. MATERIAL AND METHODS

2.1 Materials

BT nanoparticles with an average diameter of the order of 200 nm were purchased from Inframat. Poly(vinylidene fluoride) (PVDF, Kynar® grade 720) was provided by Arkema. N,N dimethylacetamide (DMAc) was purchased from Sigma-Aldrich.

2.2 Composite elaboration

The synthesis of nitrodopamine and nanoparticle functionalization with nitrodopamine were performed according to the procedure reported previously [19] which follows the procedure described by Song *et al.* [29]. Briefly, BT particles dispersed with nitrodopamine into deionized water were stirred for 18h at 40°C, then collected by centrifugation, rinsed with water and dried under vacuum. Nanocomposites with functionalized nanoparticles (called BT-f in the following) were elaborated as also described in ref [19]. Briefly, PVDF was dissolved in DMAc and a fraction of BT-f nanoparticles was added. The mixture was magnetically stirred and poured into glass cups to allow solvent evaporation. The material was then melt-compounded using a twin-screw micro-extruder and compression molded into a film of 100 µm thickness. Dumbbell shaped samples were cut off in the film and stretched at a draw temperature of 90°C up to a strain $\varepsilon = 100\%$ to promote the PVDF polar β crystal phase and thus enable the polymer to display a piezoelectric response. Note that the study is focused on composites with 10 wt% BT-f content since the latter composition is fully representative of the nanoscale behavior in the loading range between 5 and 30 wt%. For the sake of comparison, the neat PVDF sample was processed under similar conditions. The composites are denoted BT0/PVDF for pristine PVDF and BT10f/PVDF for composites with 10 wt% BT-f content.

2.3 Characterization

The BT nanoparticle shape and size distribution, as well as composite morphology were investigated by field emission scanning electron microscopy (FE-SEM) using a JEOL JSM-7800F LV equipment operated at an acceleration voltage of 3 kV and 15 kV

respectively. The samples were coated with carbon prior to performing microscopy analysis.

X-ray diffraction particle characterizations were performed on an Ultima IV Rigaku Bragg-Brentano diffractometer (Cu K_α radiation, λ = 1.5406 Å). The diffraction scans were carried over the [15-90°] 2θ-range with a step of 0.02° and a counting time of 1s/step.

The PVDF crystal structure in composites was assessed by Fourier transform infrared (FTIR) spectroscopy. Spectra were collected in ATR mode (Attenuated Total Reflexion) with a Perkin Elmer spectrometer. Data acquisition was performed on 16 scans, the spectral resolution is 2 cm^{-1}.

The surface morphology of the stretched composites was characterized using the AFM technique in alternative contact (or Tapping™) mode. The nanoscale piezoelectric and ferroelectric responses were probed by using the dual AC resonance tracking (DART) method [30] of the PFM technique in environment conditions by using a MFP-3D (Asylum Research/Oxford Instruments, USA) microscope. Pt/Ir-coated silicon tips and cantilevers with a stiffness of about 4 $N.m^{-1}$ were used as the conductive probe. More specifically, PFM imaging was used by applying AC probing voltage to the AFM tip to detect spontaneous electromechanical and switching responses of the samples, while poling experiments were performed by firstly applying high DC voltage to locally manipulate the domains. PFM in spectroscopic mode was used by recording remnant piezoresponse loops (at zero bias) after a continuous AC signal superimposed on an intermittent DC bias voltage was applied to the samples to promote electromechanical response at the expense of the electrostatic contribution [31].

3. RESULTS AND DISCUSSION

The SEM observation of BT nanoparticles is reported in Fig. 1a. The particles present a size distribution from 100 to 340 nm with an average diameter of 190 nm. Fig. 1b shows the powder X-ray diffraction pattern of the BT powder and peak indexation from the phase identification. It reveals that the crystal structure is tetragonal (P4mm space group n°99 a = 3.999 Å = b; c = 4.034 Å, ICSD card n°67520), as expected, thus suggesting piezoelectric behavior.

The crystal phase of PVDF in composites was analyzed by FTIR spectroscopy. The spectra are presented in Fig. 2a. The unstretched BT0/PVDF exhibits three characteristic bands at 766, 795 and 976 cm^{-1} associated to the non-polar PVDF α-phase (Fig. 2a(1)). As expected, after drawing, the signature of PVDF polar β-phase is confirmed by the presence of new bands at 840 and 1279 cm^{-1} in both BT0/PVDF and BT10f/PVDF composites (Figs. 2a(2) and (3)), thus confirming the electroactive capacity of the stretched polymer matrix.

SEM observations of the BT10f/PVDF surface are presented in Fig. 2b. The high applied voltage allows to probe a large interaction volume of the composite. BT-f nanoparticles appear homogeneously distributed in the PVDF matrix. Moreover nanoparticle functionalization results in a good interfacial adhesion between the ceramic nanoparticles and the polymer matrix. The latter results from local interactions in nanocomposites in which the catechol group of nitrodopamine grafts to BT nanoparticles to form a metalocycle and in the meantime the nitro group interacts with PVDF by hydrophobic – hydrophobic interaction. The stretching process does not induce any cavitation and a polymer layer around the BT particles is always visible, as illustrated in Fig. 2b(2). Such evidence for a strong interfacial resistance and an uniform functionalization around particles has already been reported in previous work [19].

The surface morphologies (AFM height images) of the BT0/PVDF and BT10f/PVDF samples are shown in Fig. 3a and c. At the nanoscale level, both samples display a fibrillary structure characteristic of stretched PVDF. The white arrows indicate the stretching direction. The root mean square surface roughness measured over 60×60µm² scan area is 540 and 460 nm for BT0/PVDF and BT10f/PVDF, respectively. These high values reflect the mechanical stretching process undergone by the samples. Figs. 3b and 3d display a zoom-in to the previous images showing crystalline blocks resulting from the fragmentation process of the α-crystal phase during the fibrillar transformation upon stretching. Similar AFM images have already been reported by Thomas *et al.* on stretched polybutene [32]. The occurrence of crystal fragmentation is in agreement with the description of the plastic deformation mechanism in PVDF as described in ref [33]. Crystal fragments are larger in BT10f/PVDF than in the case of BT0/PVDF. The difference may arise from the good interfacial adhesion between the functionalized particles and the polymer matrix which limits lamellar fragmentation. Overall no evidence for cavitation is provided. Moreover, the AFM image does not show the presence of any particles at the extreme surface of the BT10f/PVDF composite suggesting a continuous PVDF coating as previously observed at the mesoscale by SEM (Fig. 2b(2)).

The electromechanical performances of the BT/PVDF piezocomposites were then evaluated. In a previous study, the macroscopic piezoelectric coefficient d_{33} was found to be –6 pC/N for the stretched BT10f/PVDF composite [19]. The negative sign of d_{33} is indicative of the fact that the polymer matrix dominates the macroscopic piezoelectric activity at such BT content. To better understand the role played by the nanofillers on the

resulting piezo-activity of the composites, direct probing of the BT particles embedded into the matrix is required. Thus, as a first step PFM measurements in imaging mode were performed on the composites. Figs. 4b and c show the out-of-plane (OP) amplitude and phase PFM images recorded over the surface of the BT0/PVDF film in the pristine state by applying an AC voltage of 3 V. Several contrasts are observed from both amplitude and phase signals suggesting piezoelectricity and ferroelectric activity into the PVDF matrix. These features are in agreement with the presence of the polar β-phase induced by the mechanical stretching of the original α-phase, as already proven by FTIR analysis (Fig. 2a(2)). Figs. 4e and f present OP amplitude and phase PFM pattern measured on the BT10f/PVDF composite under the same applied AC probing voltage conditions. Strong piezoelectric active regions are detected, as clearly evidenced by the bright contrasts seen over the scanned area on the amplitude pattern. The associated phase signal show different contrasts, indicating various ferroelectric polarization directions. For clarity, a zoom of a specific bright region is depicted in Fig. 4h. The bright contrast seen on the PFM phase signal (Fig. 4i) and associated to the same area reveals a polarization component oriented upwards relative to the sample surface. The lateral sizes of these highly electroactive heterogeneities are in the range 100 - 300 nm. Interesting is the nonexistence of such nanoscale features on the corresponding AFM topographies shown in Figs. 4d and 4g, which rules out a morphological correspondence to such PFM contrasts. Comparison of the profile curves of the AFM topography with the associated PFM amplitude signal shown in Fig. 4j further confirms the absence of correlation. Moreover, since areas surrounding these highly electroactive zones display amplitude and phase signal levels similar to those of the BT-free sample (Figs. 4b and c), it may be concluded that these neighboring regions are the β-crystal phase of PVDF. Therefore, this β-PVDF matrix is not responsible for the particular strong enhancement

of the PFM activity. We may thus assume that BT nanoparticles lying just below the surface and coated by a thin PVDF layer are probed by the PFM tip. Such below surface inclusions, as previously observed in Fig. 4e, would account for the strong electromechanical activity. According to this assumption, the superficial polymer layer prevents the direct observation of the nanoparticle from the AFM topographic signal whereas the PFM technique, owing to the very high electric field beneath the tip, allows for the detection of its electroactive response. Larger as-grown OP piezoresponse of the ceramic inclusions compared to the surrounding piezo-polymer matrix was previously reported [27] but not with such a high level of deformation for these particles. This behavior may be explained by the interfacial cohesion improved by nitrodopamine functionalization of the BT fillers, allowing for greater efficiency of the stress transfer [19] in the present study. Moreover, in ref [27] the piezoelectric ceramic fillers embedded in P(VDF-TrFE) matrix presented micrometric size compared to our nanosized particles, and they were directly visible on the AFM topography image.

Furthers investigations were undertaken to unambiguously attribute the origin of these highly active piezoelectric regions to the presence of BT nanoparticles. First, PFM piezoloops in remnant mode were measured over the surface of the BT10f/PVDF composite both in the areas previously identified and around them. The typical recorded PFM phase and amplitude loops are illustrated in the Figs. 4k and l. Regardless of the probed region, the amplitude signal shows a well-defined butterfly-shape in relation to the inverse piezoelectric effect (Fig. 4k), while the phase piezoresponse loops display an hysteretic response with two opposite polarization states (Fig. 4l). These results confirm the local piezoelectric and ferroelectric capability of the BT10f/PVDF composite, as previously revealed by the PFM imaging contrasts. It is worth noting that the coercive voltage V_c is very different depending on the probed area. Indeed, by placing the tip over

a bright area, marked by the green cross on the PFM image in Fig. 4h, the measured V_c is about 22 V, whereas a value of the order of 42 V is determined when probing the regions outside bright features (marked by the red cross on the Fig. 4h). This higher V_c voltage value needed to switch the polarization is in good agreement with the presence of a ferroelectric polymer compound for which the bulk coercive field is known to be large (50 MV/m) [34]. In fact, in conventional inorganic piezo-/ferroelectric compounds such as BT, the reversal polarization is due to the ionic displacement, while a rotation of the molecular chains occurs in ferroelectric organic materials. Such an opening loop was also obtained on BT0/PVDF, meaning that a similar response of the PVDF β-phase occurs regardless of the presence or not of ceramic particles. Furthermore, it is worth noting that in addition to the β polar crystal regions, non-polar PVDF components (*i.e.* α-phase and amorphous) coexist, corroborating the FTIR results previously reported in Fig. 2a. Thus the complex nature of the probed volume under the tip may also explain the difficulty to efficiently switch the β crystalline lamellae by the electrical field. The much lower V_c value measured on the bright regions in Fig. 4e may be associated to more homogeneous crystalline structure, as it is the case for a piezoelectric inorganic compound. Furthermore, the piezoelectric loops exhibiting the higher deformation amplitude are the ones recorded over the bright regions, as demonstrated by the amplitude loop presented on the Fig. 4k corresponding to the location highlighted by the green cross on the PFM amplitude image. Indeed, approximately twice as much piezoelectric deformation is measured under similar probing AC voltage (V_{AC} = 3 V). In this context, although reliable values of piezoelectric coefficient determined by PFM technique are difficult to assess (complicated calibration procedure, inhomogeneous field beneath the tip, poor surface/tip contact, laser spot position, AFM probe nature, …), comparison of the relative values deduced from the amplitude loops may be done with confidence since all PFM

loops were acquired the same day under similar experimental conditions. As a consequence, through these local spectroscopic measurements, we can reasonably attribute the highly active piezoelectric zones to the BT nanoparticle inclusions into the polymer matrix.

Further investigations of the polarization switching behavior were achieved by means of poling experiments on both BT0/PVDF and BT10f/PVDF samples. First, a stretched pristine PVDF layer was probed in PFM imaging mode and the results are presented in Figs. 5a-c. Then, a 3×3 µm² selected area was scanned by applying ±130 V to the probing tip (see dashed square zones in Fig. 5d). As seen on Fig. 5f, clear opposite bright and dark contrasts are obtained for the OP PFM phase signal, related to the upwards and downwards polarization respectively. These contrasts confirm the polar state of the probed PVDF region, in agreement with the presence of the PVDF β-phase assessed in Fig. 2a(2), and demonstrate the efficiency of the ferroelectric switching phenomena in such stretched PVDF layer. Only a few areas are not fully polarized which are mainly attributed to the amorphous fraction and/or to the remaining fraction of α-crystal phase. Corresponding OP PFM amplitude image depicted on Fig. 5e reveals strong deformation for the two created domains, as evidenced by the very bright contrasts. This is due to the specific orientation of the hydrogen and fluorine atoms along the carbon chain axis which promotes higher deformation in the OP direction. Whatever the direction of the polarization vector (namely upwards or downwards), the piezoelectric vibration amplitude detected by the tip presents similar values suggesting relatively homogeneous electromechanical behavior of the sample. Domain walls seem to be identified by the fall of the piezosignal due the to the change in polarization between the two polarized regions (highlighted by blue arrows), but these areas are larger than typical domain walls previously detected by PFM in fluoropolymers [35]. The written domains seem to be

limited by the crystalline blocks. Indeed, as revealed on Fig. 5f, zones of uniform polarizations are irregular and are correlated to the surface features where distinct nanosized crystals fragments are observed (Fig. 5d) suggesting a single crystalline block switching. Thus, although both modification of conformation and dipole rotation around the PVDF chain are linked, owing to the covalent bonding of the chains, the nanometric probing tip from which the electric field is induced allows to polarize an unique crystalline block (previously described) without switching the polarization of the nearby fragments, as already reported by Rodriguez *et al.* [36].

Then poling experiments were conducted on the specific areas of the BT10f/PVDF nanocomposite where the presence of BT particles was highlighted by PFM imaging. A DC electric pulse was applied in order to investigate the local switching of the polarization. The OP PFM amplitude and phase signals in the as-grown state simultaneously recorded with the surface morphology are presented in Figs. 6a-c. Application of +70 V voltage pulse at the location indicated by the blue cross on the Fig. 6d leads to a clear change in PFM phase contrast, namely from dark (Fig. 6c) to bright (after applied pulse, Fig. 6f) contrast, revealing the OP switching of polarization inside the BT particle. Subsequent application of a negative pulse (–70 V) induces a back-switching of the polarization, as demonstrated by the dark contrast obtained on the PFM phase response in Fig. 6i similar to that observed for the original un-poled state. The corresponding vibration amplitude images show only bright contrast (Figs. 6b, e and h) which means that homogeneous piezoelectric deformation occurs regardless of the upwards or downwards polarization state. Besides, we note that the switching phenomenon is spatially confined to the nano-region previously assigned to the inorganic particle, further confirming detection of the BT particles. This result demonstrates the ability to identify nanometric inorganic materials embedded into a polymer matrix by

means of the contact PFM method. Also, the voltage needed to fully switch the polarization into the BT particle is much lower than the one required in the neat PVDF phase (70 V *vs.* 130 V, respectively) which is in agreement with the piezoresponse loops previously presented and expected for such ferroelectric ceramic and polymer systems. The nanometric size (*i.e.* about 340×270 nm²) and the irregular shape of the manipulated regions compare well with SEM data obtained on BT powder as shown in Fig. 1a, thus attesting the accurate detection of such piezoelectric particles by PFM technique and the local control of their ferroelectric polarization by poling. This had not been evidenced by KPFM in the work of Shvartsman *et al.* where higher inorganic grain sizes (~1 µm) were incorporated into the polymer matrix [23]. This result is significant considering: i) the nanosized powder of our particles (about 190 nm), ii) the relatively low BT particle content (10 wt% *vs.* 40 vol% in [23]), iii) the presence of the particles beneath the sample surface, and iv) the very low dielectric constant of the PVDF matrix (about 10) as compared to the BT compound (about 2000). Indeed, in the latter case the fillers are submitted to an effective field much lower than the electric field induced by the AFM tip, resulting in a decrease of the piezoelectric response (although one must keep in mind the much higher piezoelectric coefficient of the BT particles as compared to that of PVDF, d_{33} ~100 pC.N^{-1} *vs.* $|d_{33}|$ ~30 pC.N^{-1} [37]).

As a result, though PFM is a contact method, our results demonstrate its sufficient sensitivity to evidence nanosized inorganic particles dispersed into a polymer matrix, even in the particular case of complex stretched systems. This direct visualization of the inclusions combined to their well-controlled ferroelectric polarization will allow to

accurately determine the contribution of such nanofillers to the macroscopic performance of the future piezocomposites systems.

4. CONCLUSIONS

We have investigated the local piezoelectric and ferroelectric behavior of electroactive nanocomposites made of functionalized BT nanoparticles dispersed into a PVDF matrix by means of the PFM technique. A stretching step was performed to promote the PVDF β polar crystal phase in the film, as confirmed by FTIR analysis. An homogeneous distribution of BT particles into the polymer combined to a good interfacial adhesion between both components was obtained thanks to nitrodopamine functionalization. The AFM surface morphology investigation has shown the nanometric crystalline blocks resulting from the fragmentation of crystalline lamellae upon drawing. PFM experiments have shown piezo-activity of pristine PVDF film in agreement with the presence of the β polar phase induced mechanically. In addition, local poling tests have revealed the efficiency of the ferroelectric switching phenomena in such stretched PVDF film. In the case of the BT10f/PVDF composite, highly piezo-active regions unlike those of the surrounding polymer were evidenced by PFM imaging, in complete accordance both in size and in shape with nanosized BT fillers. Then, by precisely placing the AFM probe over these specific electromechanical zones attributed to the BT inclusions, manipulation of the ferroelectric polarization state has been successfully achieved. These results have demonstrated the ability of the PFM tool to directly image individual piezoelectric nanometric fillers embedded into a polymer matrix and to control polarization as well, allowing for in-depth study of electroactive composites on the nanoscale.

AUTHOR INFORMATION

Corresponding Author

*Anthony Ferri, E-mail : anthony.ferri@univ-artois.fr

UCCS - UMR CNRS 8181, Université d'Artois, Faculté des Sciences Jean Perrin, Rue Jean Souvraz, 62307 Lens, France

ACKNOWLEDGMENTS

This work was partly supported through grant ANR-16-CE08-0025, ANR NanoPiC from French National Research Agency. Région Hauts-de-France and Fonds Européen de Développement Régional (FEDER) are gratefully acknowledged for funding the MFP-3D microscope under Program "Chemistry and Materials for a Sustainable Growth". The FE-SEM equipment have been implemented at the electron microscope facility (Institut Chevreul) thanks to the financial support of Région Hauts-de-France and FEDER. Technical assistance from Dr. Ahmed Addad and Dr. Alexandre Fadel is gratefully acknowledged.

REFERENCES

[1] J. Yao, C. Xiong, L. Dong, C. Chen, Y. Lei, L. Chen, R. Li, Q. Zhu, X. Liu, Enhancement of dielectric constant and piezoelectric coefficient of ceramic–polymer composites by interface chelation. J. Mater. Chem. 19 (2009) 2817-2821. https://pubs.rsc.org/en/content/articlehtml/2009/jm/b819910h.

[2] J. Li, J. Claude, L.E. Norena-Franco, S. Il Seok, Q. Wang, Electrical Energy Storage in Ferroelectric Polymer Nanocomposites Containing Surface-Functionalized $BaTiO_3$ Nanoparticles. Chem. Mater. 20 (2008) 6304-6306. https://pubs.acs.org/doi/10.1021/cm8021648.

[3] Z.-M. Dang, J.-K. Yuan, J.-W. Zha, T. Zhou, S.-T. Li, G.-H. Hu, Fundamentals, processes and applications of high-permittivity polymer-matrix composites. Prog. Mater. Sci. 57 (2012) 660-723. https://doi.org/10.1016/j.pmatsci.2011.08.001.

[4] T. Furukawa, K. Ishida, E. Fukada, Piezoelectric properties in the composite systems of polymers and PZT ceramics. J. Appl. Phys. 50 (1979) 4904-4912. https://doi.org/10.1063/1.325592.

[5] B. Améduri. From vinylidene fluoride (VDF) to the applications of VDF-Containing polymers and copolymers: recent developments and future trends. Chem. Rev. 109 (2009) 6632-86. https://pubs.acs.org/doi/10.1021/cr800187m.

[6] A.J. Lovinger, Annealing of poly(vinylidene fluoride) and formation of a fifth phase. Macromolecules 15 (1982) 40-44. https://pubs.acs.org/doi/10.1021/ma00229a008.

[7] T. Furukawa, Ferroelectric properties of vinylidene fluoride copolymers. Phase Transitions 18 (1989) 143-211. https://www.tandfonline.com/doi/abs/10.1080/01411598908206863.

[8] P. Martins, A. C. Lopes, S. Lanceros-Mendez, Electroactive phases of poly(vinylidene fluoride): Determination, processing and applications. Prog. Polym. Sci. 39 (2014) 683-706. https://doi.org/10.1016/j.progpolymsci.2013.07.006.

[9] J. Gomes, J. Serrado Nunes, V. Sencadas, S. Lanceros-Mendez, Influence of the β-phase content and degree of crystallinity on the piezo- and ferroelectric properties of poly(vinylidene fluoride). Smart Mater. Struct. 19 (2010) 065010. https://iopscience.iop.org/article/10.1088/0964-1726/19/6/065010.

[10] D. Mandal, K. Henkel, D. Schmeißer, The electroactive β-phase formation in Poly(vinylidene fluoride) by gold nanoparticles doping. Mater. Lett. 73 (2012) 123-125. https://doi.org/10.1016/j.matlet.2011.11.117.

[11] W.C. Gan and W.H. Abd Majid, Effect of TiO_2 on enhanced pyroelectric activity of PVDF composite. Smart Mater. Struct. 23 (2014) 045026. https://iopscience.iop.org/article/10.1088/0964-1726/23/4/045026.

[12] Y.K.A. Low, L.Y. Tan, L.P. Tan, F.Y.C. Boey, K.W. Ng, Increasing solvent polarity and addition of salts promote β-phase poly(vinylidene fluoride) formation. J. Appl. Polym. Sci. 128 (2012) 2902-2910. https://onlinelibrary.wiley.com/doi/full/10.1002/app.38451.

[13] T. Soulestin, V. Ladmiral, F. Domingues Dos Santos, B. Améduri, Vinylidene fluoride- and trifluoroethylene-containing fluorinatedelectroactive copolymers. How does chemistry impact properties? Prog. Polym. Sci. 72 (2017) 16-60. https://doi.org/10.1016/j.progpolymsci.2017.04.004.

[14] K.S. Ramadan, D Sameoto, S Evoy, A review of piezoelectric polymers as functional materials for electromechanical transducers. Smart Mater. Struct. 23 (2014) 033001. https://iopscience.iop.org/article/10.1088/0964-1726/23/3/033001/meta.

[15] J.-F. Capsal, E. Dantras, L. Laffont, J. Dandurand, C. Lacabanne, Nanotexture influence of $BaTiO_3$ particles on piezoelectric behaviour of PA 11/$BaTiO_3$ nanocomposites. J. Non-Cryst. Solids 356 (2010) 629-634. https://doi.org/10.1016/j.jnoncrysol.2009.06.050.

[16] M.V. Silibin, J. Belovickis, S. Svirskas, M. Ivanov, J. Banys, A.V. Solnyshkin, S.A. Gavrilov, O.V. Varenyk, A.S. Pusenkova, N. Morozovsky, V.V. Shvartsman, A.N. Morozovska, Polarization reversal in organic-inorganic ferroelectric composites:

Modeling and experiment. Appl. Phys. Lett. 107 (2015) 142907. https://doi.org/10.1063/1.4932661.

[17] Y. Zhao, Q. Liao, G. Zhang, Z. Zhang, Q. Liang, X. Liao, Y. Zhang, High output piezoelectric nanocomposite generators composed of oriented $BaTiO_3$ NPs@PVDF. Nano Energy 11 (2015) 719-727. https://doi.org/10.1016/j.nanoen.2014.11.061.

[18] X. Chen, X. Li, J. Shao, N. An, H. Tian, C. Wang, T. Han, L. Wang, B. Lu, High-Performance Piezoelectric Nanogenerators with Imprinted P(VDF-TrFE)/$BaTiO_3$ Nanocomposite Micropillars for Self-Powered Flexible Sensors. Small 13 (2017) 1-12. https://onlinelibrary.wiley.com/doi/full/10.1002/smll.201604245.

[19] J. Defebvin, S. Barrau, J. Lyskawa, P. Woisel, J.-M. Lefebvre, Influence of nitrodopamine-functionalized barium titanate content on the piezoelectric response of poly(vinylidene fluoride) based polymer-ceramic composites. Compos. Sci. Technol. 147 (2017) 16-21. https://doi.org/10.1016/j.compscitech.2017.05.001.

[20] H.-J. Ye, W.-Z Shao, L. Zhen, Tetradecylphosphonic acid modified $BaTiO_3$ nanoparticles and its nanocomposite. Colloids Surf. A Physicochem. Eng. Asp. 427 (2013) 19-25. https://doi.org/10.1016/j.colsurfa.2013.02.068.

[21] K. Tomoaki, Y. Kang, M. Toshiyuki, A. Masatoshi, Lead-Free Piezoelectric Ceramics with Large Dielectric and Piezoelectric Constants Manufactured from $BaTiO_3$ Nano-Powder. Jpn. J. Appl. Phys. 46 (2L) (2007) L97. https://iopscience.iop.org/article/10.1143/JJAP.46.L97/meta.

[22] U. Valiyaneerilakkal and S. Varghese, Poly(vinylidene-trifluoroethylene)/barium titanate nanocomposite for ferroelectric nonvolatile memory devices. AIP Adv. 3 (2013) 042131. https://doi.org/10.1063/1.4802980.

[23] V.V. Shvartsman, D.A. Kiselev, A.V. Solnyshkin, D.C. Lupascu, M.V. Silibin, Evolution of poled state in P(VDFTrFE)/(Pb,Ba)(Zr,Ti)O_3 composites probed by

temperature dependent Piezoresponse and Kelvin Probe Force Microscopy. Sci. Rep. 8, (2018) 378. https://www.nature.com/articles/s41598-017-18838-1.

[24] D.A. Kiselev, M.D. Malinkovich, Y.N. Parkhomenko, A.V. Solnyshkin, A.A. Bogomolov, M.V. Silibin, S.A. Gavrilov, V.V. Shvartsman, D.C. Lupascu, The Microstructure and Local Piezoelectric Response in Polymer Nanocomposites with Different Ferroelectric Crystalline Additions. Mater. Res. Soc. Symp. Proc. 1556 (2013) mrss13-1556-w10-01. https://doi.org/10.1557/opl.2013.784.

[25] A. Baji, Y.-W. Mai, Q. Li, Y. Liu, Nanoscale investigation of ferroelectric properties in electrospun barium titanate/polyvinylidene fluoride composite fibers using piezoresponse force microscopy. Compos. Sci. Technol. 71 (2011) 1435-1440. https://doi.org/10.1016/j.compscitech.2011.05.017.

[26] H.B. Kang, C.S. Han, J.C. Pyun, W.H. Ryu, C.Y. Kang, S.C. Yong, (Na,K)NbO_3 nanoparticle-embedded piezoelectric nanofiber composites for flexible nanogenerators. Compos. Sci. Technol. 111 (2015) 1-8. https://doi.org/10.1016/j.compscitech.2015.02.015.

[27] M.V. Silibin, A.V. Solnyshkin, D.A. Kiselev, A.N. Morozovska, E.A. Eliseev, S.A. Gavrilov, M.D. Malinkovich, D.C. Lupascu, V.V. Shvartsman, Local ferroelectric properties in polyvinylidene fluoride/barium lead zirconate titanate nanocomposites: Interface effect. J. Appl. Phys. 114 (2013) 144102. https://doi.org/10.1063/1.4824463.

[28] X. Hu, X. Yan, L. Gong, F. Wang, Y. Xu, L. Feng, D. Zhang, Y. Jiang, Improved Piezoelectric Sensing Performance of P(VDF−TrFE) Nanofibers by Utilizing BTO Nanoparticles and Penetrated Electrodes. ACS Appl. Mater. Interfaces 11 (2019) 7379-7386. https://pubs.acs.org/doi/pdf/10.1021/acsami.8b19824.

[29] Y. Song, Y. Shen, H. Liu, Y. Lin, M. Lia, C.-W. Nan, Improving the dielectric constants and breakdown strength of polymer composites: effects of the shape of the

$BaTiO_3$ nanoinclusions, surface modification and polymer matrix. J. Mater. Chem. 22 (2012) 16491-16498. https://pubs-rsc-org.inc.bib.cnrs.fr/en/content/articlelanding/2012/JM/c2jm32579a#!divAbstract.

[30] B.J. Rodriguez, C. Callahan, S.V. Kalinin, R. Proksch, Dual frequency resonance-tracking atomic force microscopy. Nanotechnology 18 (2007) 475504. https://iopscience.iop.org/article/10.1088/0957-4484/18/47/475504/meta.

[31] S. Kim, D. Seol, X.L. Lu, M. Alexe, Y. Kim, Electrostatic-free piezoresponse force microscopy. Sci. Rep. 7 (2017) 41657. https://www.nature.com/articles/srep41657.

[32] C. Thomas, R. Seguela, F. Detrez, V. Miri, C. Vanmansart, Plastic deformation of spherulitic semi-crystalline polymers: An in situ AFM study of polybutene under tensile drawing. Polymer 50 (2009) 3714-3723. https://doi.org/10.1016/j.polymer.2009.06.023.

[33] J. Defebvin, S. Barrau, G. Stoclet, C. Rochas, J.M. Lefebvre, In situ SAXS/WAXS investigation of the structural evolution of poly(vinylidene fluoride) upon uniaxial stretching. Polymer 84 (2016) 148-157. https://doi.org/10.1016/j.polymer.2015.12.041.

[34] V.M. Fridkin and S. Ducharme, General features of the intrinsic ferroelectric coercive field. Phys. Solid State 43 (2001) 1320-1324. https://link.springer.com/article/10.1134/1.1386472.

[35] P. Sharma, T.J. Reece, S. Ducharme, A. Gruverman, High-Resolution Studies of Domain Switching Behavior in Nanostructured Ferroelectric Polymers. Nano Lett. 11 (2011) 1970-1975. https://pubs.acs.org/doi/abs/10.1021/nl200221z.

[36] B.J. Rodriguez, S. Jesse, S.V. Kalinin, J. Kim, S. Ducharme, V.M. Fridkin, Nanoscale polarization manipulation and imaging of ferroelectric Langmuir-Blodgett polymer films. Appl. Phys. Lett. 90 (2007) 122904. https://doi.org/10.1063/1.2715102.

[37] T.D Usher, K.R Cousins, R. Zhang, S. Ducharme, The promise of piezoelectric polymers. Polym. Int. 67 (2018) 790-798. https://onlinelibrary.wiley.com/doi/10.1002/pi.5584.

FIGURE CAPTIONS

Fig. 1. Characterization of the BT particles. (a) SEM image of commercial BT particles and (b) powder X-ray diffractogram on tetragonal BT nanoparticles.

Fig. 2. Structural characterization of the composites. (a) FTIR spectra of (1) unstretched BT0/PVDF, (2) stretched BT0/PVDF and (3) stretched BT10f/PVDF composites. (b) SEM image at 15 kV of the surface of stretched BT10f/PVDF composite at 2 different magnifications: (1) ×1000 and (2) ×10000 (stretching direction is horizontal).

Fig. 3. Surface morphology of the stretched samples. AFM morphologies of (a, b) BT0/PVDF and (c, d) BT10f/PVDF composites recorded over 60×60 µm² and 5×5 µm² scan regions. White arrows refer to the stretching direction.

Fig. 4. Local electromechanical activity of the samples. Images of the (a, d, g) AFM topography, PFM (b, e, h) amplitude and (c, f, i) phase signals for the (a-c) BT0/PVDF and the (d-i) BT10f/PVDF composites. The profiles curves of the AFM topography and the PFM amplitude corresponding to the dashed yellow lines are shown in (j), showing no-correlation between both signals. Remnant PFM loops (k) in amplitude and (l) in phase recorded over the surface of the BT10f/PVDF sample. The red and green crosses in the PFM amplitude image presented in (h) refer to the red and green piezoresponse loops, respectively. The scan size is 5×5 µm² for (a-f) and 1×1 µm² for (g-i).

Fig. 5. Local manipulation of the ferroelectricity in the pristine PVDF sample. Topography (a), PFM amplitude (b) and PFM phase (c) images in the as-grown state, and topography (d), PFM amplitude (e) and PFM phase (f) images after applying ±130 V in order to create artificial domains into the BT0/PVDF sample. Blue arrows in (e) show the created domain wall. The scan size is 5×5 μm^2.

Fig. 6. Local manipulation of the ferroelectricity in BT10f/PVDF composite. Topography (a), PFM amplitude (b) and PFM phase (c) images in the as-grown state. Topography (d), PFM amplitude (e) and PFM phase (f) images after applying a DC pulse of +70 V at the location symbolized by the blue cross in (d). Topography (g), PFM amplitude (h) and PFM phase (i) images after applying subsequently a DC pulse of –70 V at the same location indicated in (d). The specific PFM contrasts evidence the reversible and confined switching of the polarization inside the inorganic particle. The scan size is 500×500 nm^2.

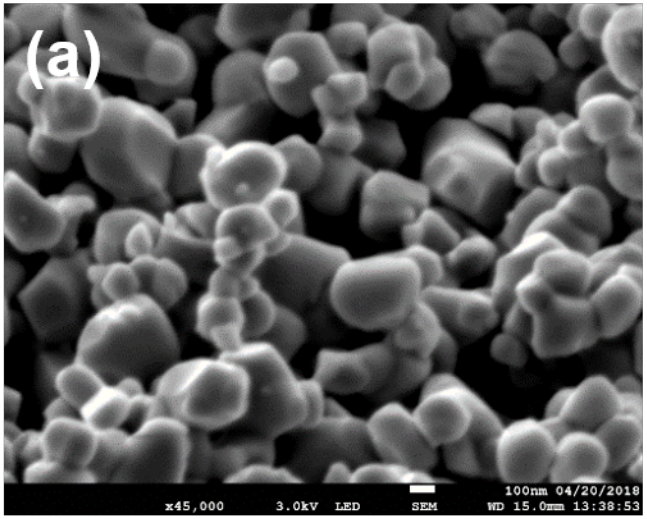
(a)
x45,000 3.0kv LED SEM 100nm 04/20/2018 WD 15.0mm 13:38:53

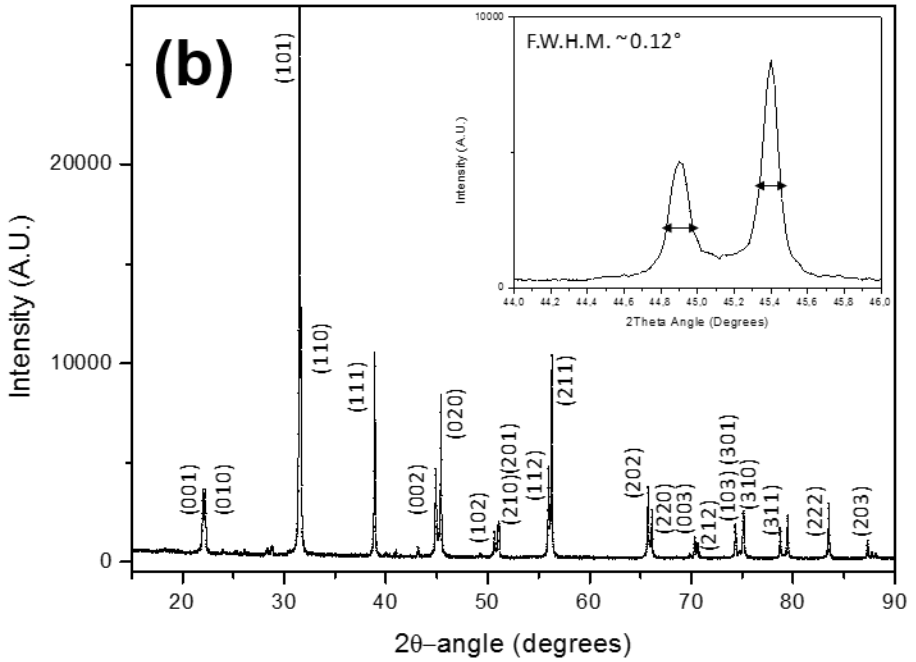
(b)
Intensity (A.U.)
2θ–angle (degrees)
(001)
(010)
(101)
(110)
(111)
(002)
(020)
(102)
(210)(201)
(112)
(211)
(202)
(220)
(003)
(212)
(103)(301)
(310)
(311)
(222)
(203)
F.W.H.M. ~0.12°
Intensity (A.U.)
2Theta Angle (Degrees)

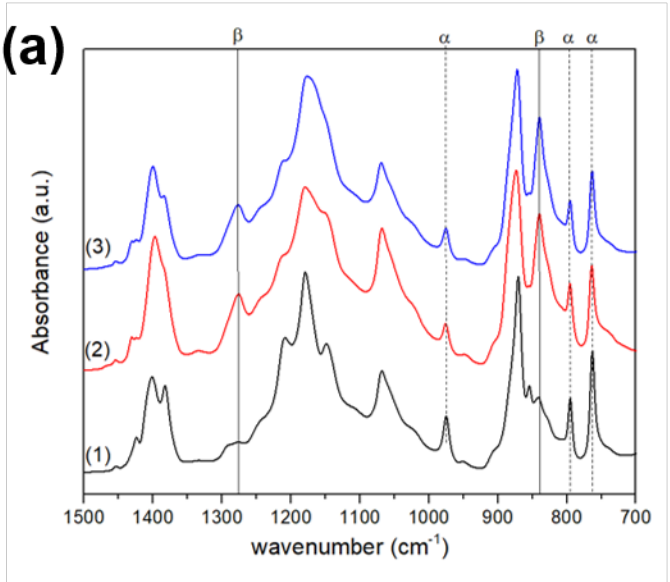
(a)
β
α
β
α
α
(3)
(2)
(1)
Absorbance (a.u.)
1500
1400
1300
1200
1100
1000
900
800
700
wavenumber (cm-1)

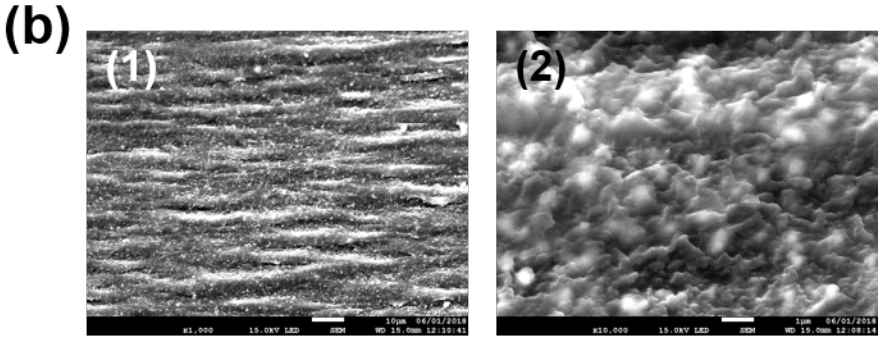
(b)
(1)
(2)

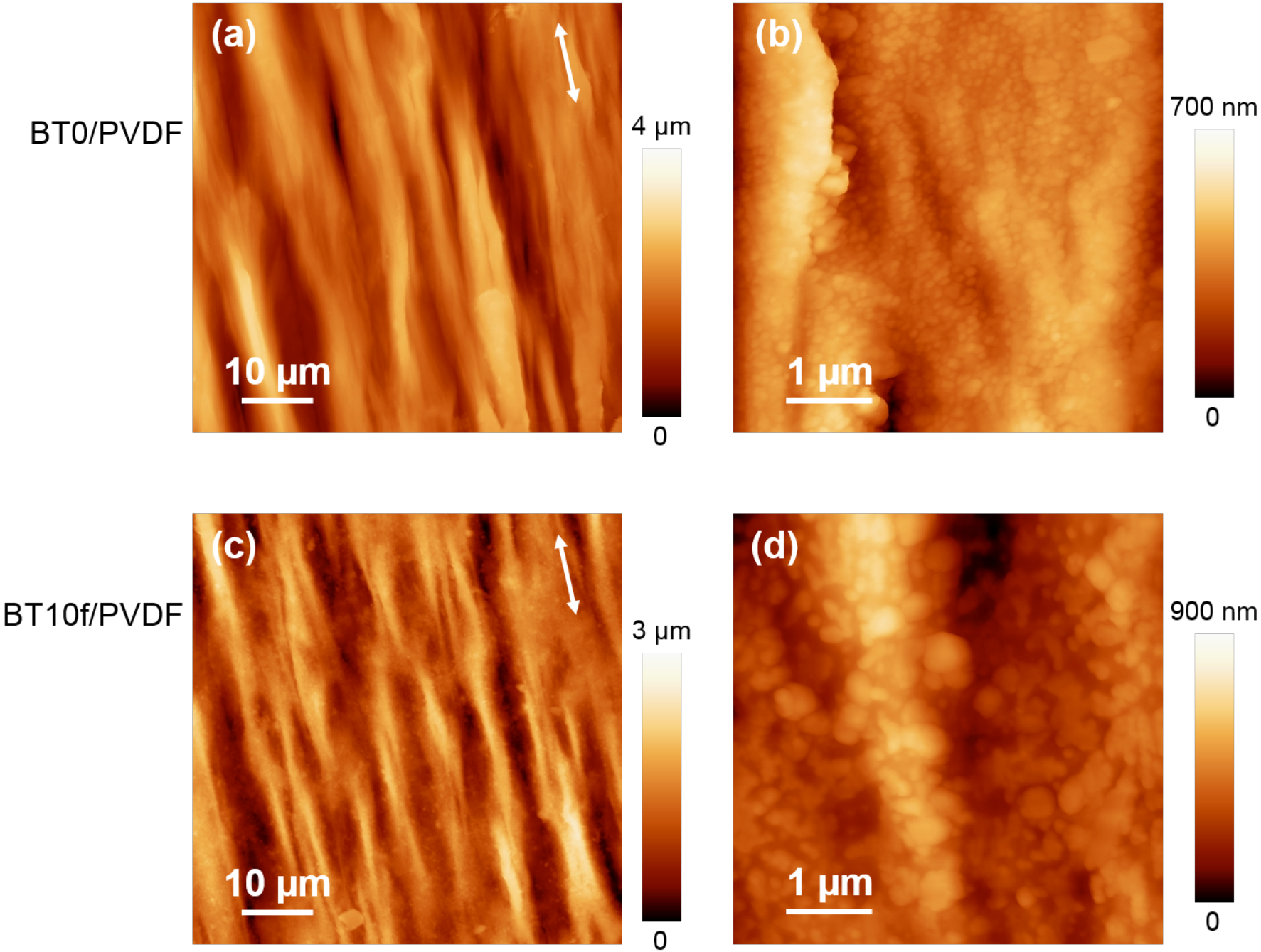
BT0/PVDF
(a)
10 μm
4 μm
0
(b)
1 μm
700 nm
0
BT10f/PVDF
(c)
10 μm
3 μm
0
(d)
1 μm
900 nm
0

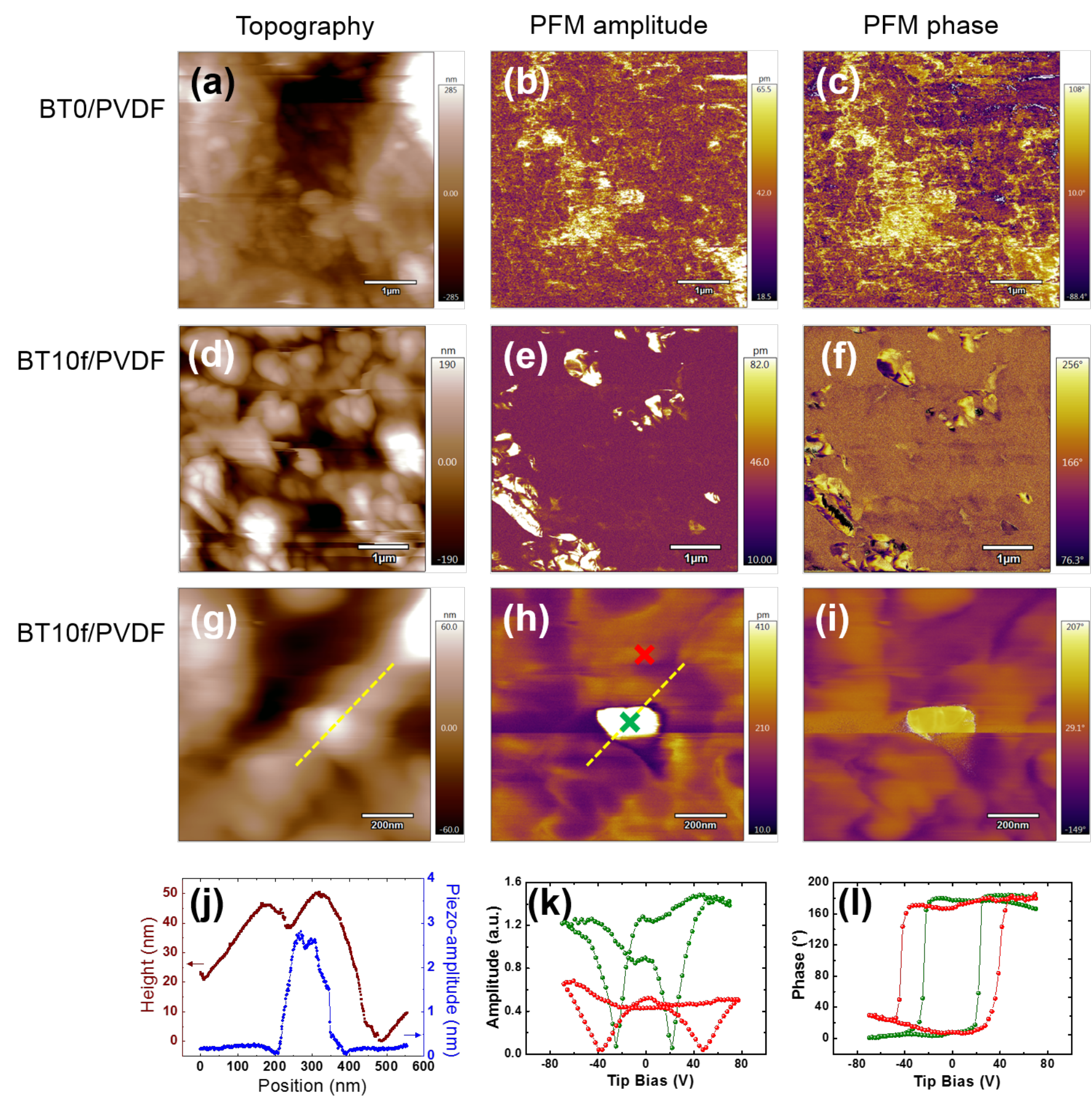
Topography
PFM amplitude
PFM phase
BT0/PVDF
BT10f/PVDF
BT10f/PVDF
(a)
(b)
(c)
(d)
(e)
(f)
(g)
(h)
(i)
(j)
(k)
(l)
nm
285
0.00
-285
pm
65.5
42.0
18.5
108°
10.0°
-88.4°
190
-190
82.0
46.0
10.00
256°
166°
76.3°
60.0
-60.0
410
210
10.0
207°
29.1°
-149°
1μm
200nm
Height (nm)
Piezo-amplitude (nm)
Position (nm)
Amplitude (a.u.)
Tip Bias (V)
Phase (°)
Tip Bias (V)

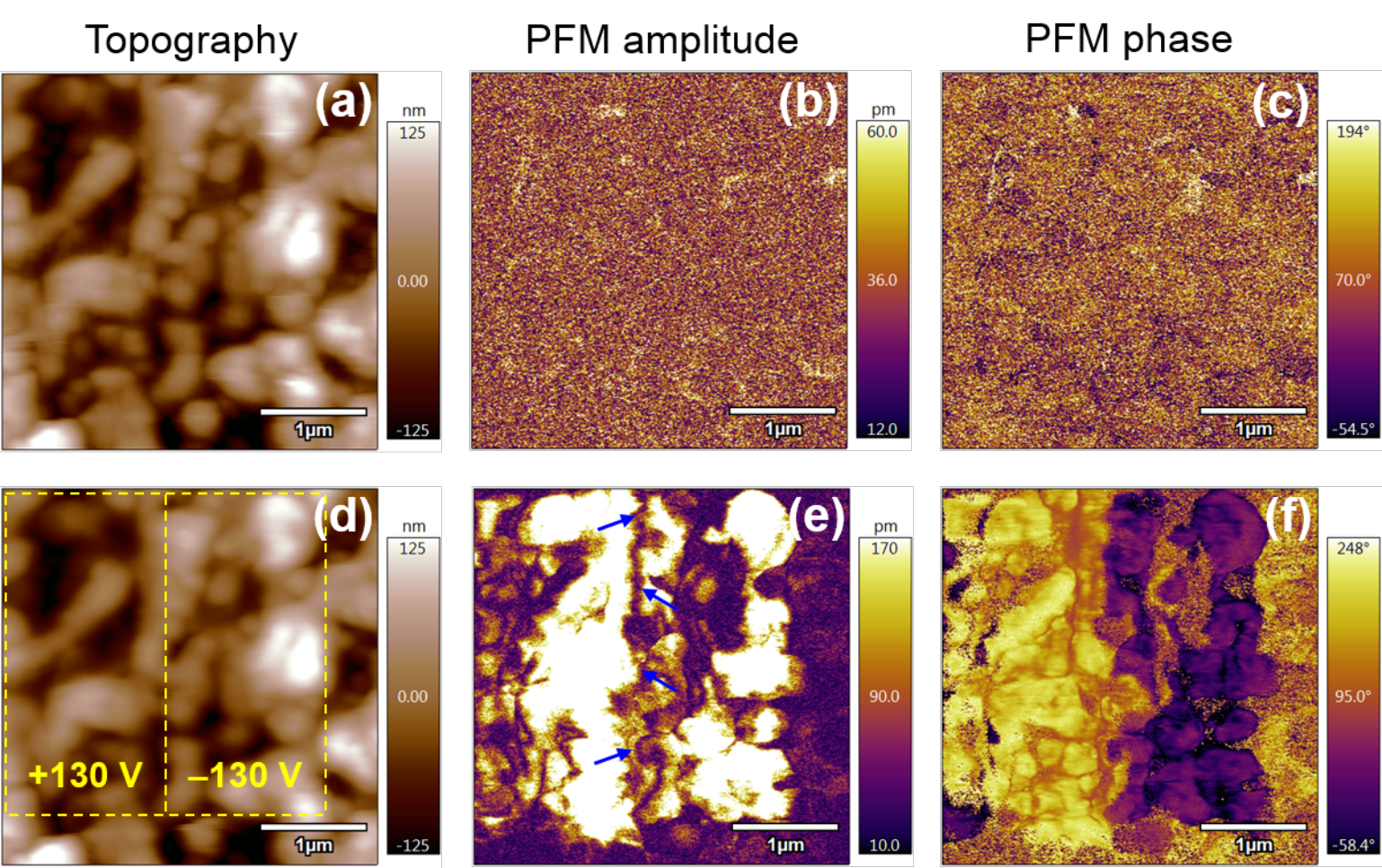
Topography
PFM amplitude
PFM phase
(a)
nm
125
0.00
-125
1μm
(b)
pm
60.0
36.0
12.0
1μm
(c)
194°
70.0°
-54.5°
1μm
(d)
nm
125
0.00
-125
+130 V
–130 V
1μm
(e)
pm
170
90.0
10.0
1μm
(f)
248°
95.0°
-58.4°
1μm

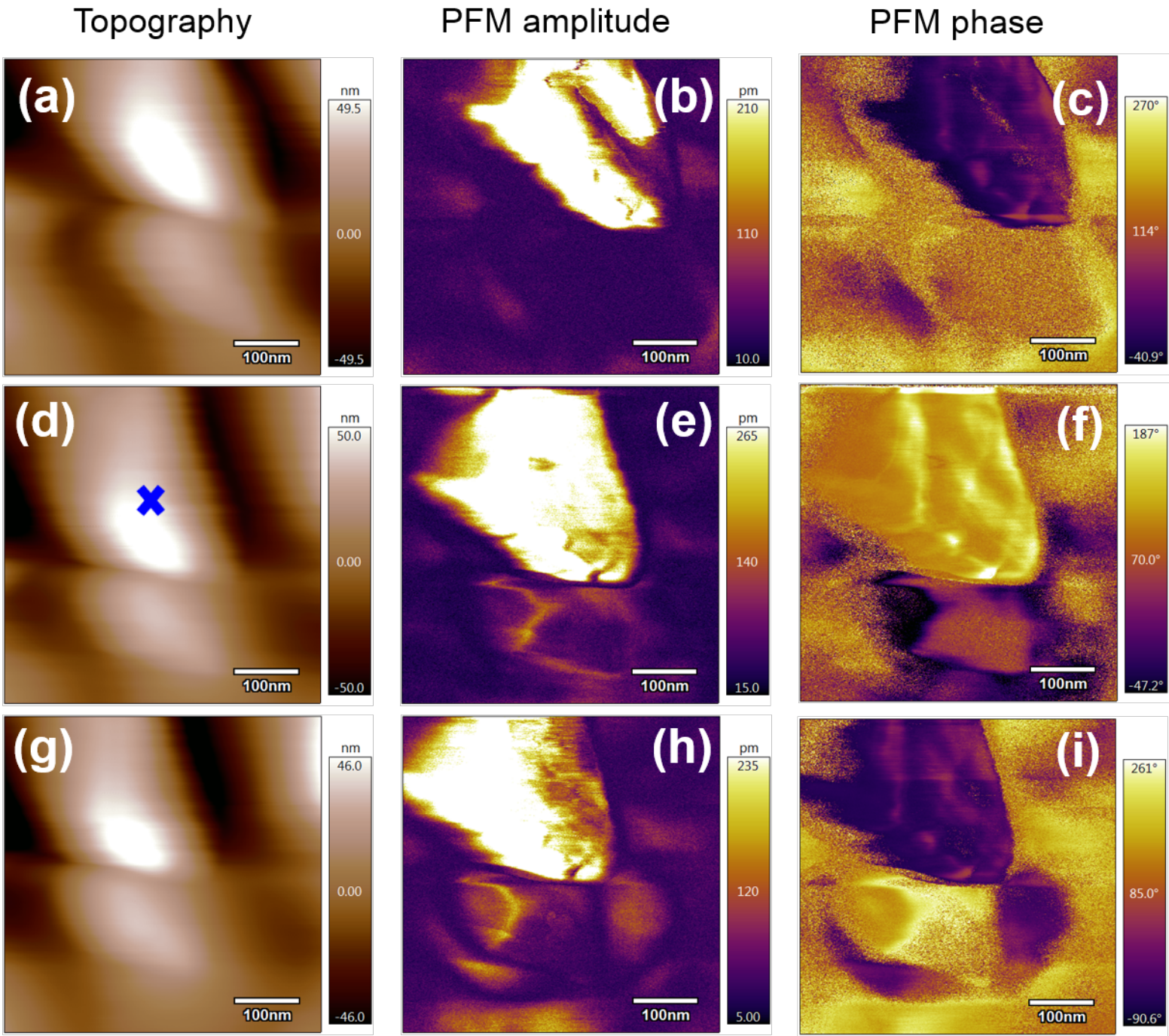
Topography
PFM amplitude
PFM phase
(a)
nm
49.5
0.00
-49.5
100nm
(b)
pm
210
110
10.0
100nm
(c)
270°
114°
-40.9°
100nm
(d)
nm
50.0
0.00
-50.0
100nm
(e)
pm
265
140
15.0
100nm
(f)
187°
70.0°
-47.2°
100nm
(g)
nm
46.0
0.00
-46.0
100nm
(h)
pm
235
120
5.00
100nm
(i)
261°
85.0°
-90.6°
100nm